Contents lists available at ScienceDirect

Journal of Colloid and Interface Science

journal homepage: http://ees.elsevier.com

Regular Article

Multi-axis alignment of Rod-like cellulose nanocrystals in drying droplets

Cailean Q. Pritchard[a,b], Fernando Navarro[b], Maren Roman[b,c,*], Michael J. Bortner[a,b,*]

[a] Department of Chemical Engineering, Virginia Tech, 245 Goodwin Hall, 635 Prices Fork Road, Blacksburg, VA 24061, United States
[b] Macromolecules Innovation Institute, Virginia Tech, Blacksburg, VA 24061, United States
[c] Department of Sustainable Biomaterials, Virginia Tech, Blacksburg, VA 24061, United States

ARTICLE INFO

Article history:
Received 15 February 2021
Received in revised form 10 June 2021
Accepted 11 June 2021
Available online xxx

Keywords
Evaporation-induced self-assembly
Cellulose nanocrystal
CNC
Rigid rod
Radial alignment
Tangential alignment
PLM

ABSTRACT

Hypothesis: Radial capillary flow in evaporating droplets carry suspended nanoparticles to its periphery where they are deposited and form a coffee-ring. Rod-like nanoparticles seeking to minimize their capillary energy will align with their long-axis parallel to the contact line. Particles exhibiting electrostatic repulsion, such as cellulose nanocrystals (CNCs), establish a competition between capillary flow-induced impingement against a growing coffee-ring and entropic minimization leading to enhanced particle mobility. Therefore, balancing these effects by manipulating the local particle concentration in drying droplets should result in deposition with a controlled orientation of CNCs.

Experiments: The dynamic local order in aqueous suspensions of CNCs in evaporating sessile droplets was investigated through time-resolved polarized light microscopy. The spatial distribution of alignment in deposited CNCs was explored as a function of nanoparticle concentration, droplet volume, initial degree of anisotropy, and substrate hydrophobicity. Computational analysis of the rotational Péclet number during evaporation was also investigated to evaluate any effects of shear-induced alignment.

Findings: Multiple modes of orientation were identified suggesting local control over CNC orientation and subsequent properties can be attained via droplet-based patterning methods. Specifically, high local particle concentrations led to tangential alignment and lower local particle concentrations resulted in new evidence for radial alignment near the center of dried droplets.

1. Introduction

Droplets of colloidal suspensions that dry on non-absorbing, solid surfaces are ubiquitous phenomena. Coffee stains on table surfaces and water stains on kitchen and bathroom fixtures are two familiar examples of the ensuing particle deposits. Accordingly, evaporating sessile droplets commonly exhibit radial flow within the droplet while drying which carry suspended particles to the edge of the droplet [1–3]. Numerous investigations have sought to prevent the formation of these toroidal deposits, or “coffee-rings”, in the pursuit of producing uniform films. These studies modify the solvent evaporation rate [4], induce Marangoni convection [5,6], suppress flow through gelation [7,8], or control the substrate’s surface energy [2,3] to suppress outward capillary flow. While these technologies are interesting, there has been minimal exploration of the benefits of non-uniform directed deposition methods, especially involving anisotropic nanomaterials. Anti-counterfeit coatings and patterning of nanoscale structures are excellent examples of technologies that rely on spatially non-uniform directed deposition methods and can exploit the complex fluid dynamic profiles developed in drying droplets [9–12].

Such technologies can further be developed through the use of optically and mechanically anisotropic materials such as cellulose nanocrystals (CNCs) which are rod-shaped nanoparticles that tend to organize into ordered liquid crystalline phases [13–16]. In these materials, the cellulose backbone is oriented parallel to the long-axis of the rod leading to birefringence and anisotropic mechanical properties [17]. Control over CNC orientation drives their performance as photonic crystals or smart nanomaterials, which is governed by the complex relationship between fluid transport, contact line dynamics, and interparticle interactions. To this end, evaporation-induced alignment is presented as a low energy alternative to orient CNCs and other rod shaped particles compared to conventional methods that apply magnetic [18–20], shear forces [21–23], electrospraying [24], or gas flow induced alignment [25]. In 2009, we were the first to report the coffee-ring effect for cellulose nanocrystal suspensions [26]. Mashkour et al. recently demonstrated excellent control over patterned structures of CNCs using contact line motion in evaporating CNC suspensions to im-

*Abbreviations*CNCcellulose nanocrystal.PLMpolarized light microscopy.AFMatomic force microscopy.

* Corresponding authors at: Macromolecules Innovation Institute, Virginia Tech, Blacksburg, VA 24061, United States (M. Roman and M.J. Bortner).

E-mail addresses: cqpritch@vt.edu (C.Q. Pritchard); maren.roman@vt.edu (M. Roman); mbortner@vt.edu (M.J. Bortner)

https://doi.org/10.1016/j.jcis.2021.06.069
0021-9797/© 2021.

part alignment through a surface tension torque [12,27]. Our work supports Mashkour's invocation of the surface tension torque's role in evaporation-based particle orientation and provides further insight into alternative orientation states that can be achieved through similar methods.

Here, we investigate the relative impact of flow-induced orientation compared to orientation governed by interparticle interactions and contact line motion. Computational fluid dynamic simulations were performed to analyze the rotational Péclet number which expresses the relative contribution of Brownian motion and shear forces on suspended particle alignment. Further, we identified conditions leading to the development of tangential and radial alignment through time-resolved polarized light microscopy (PLM). Additionally, an intermediate orientation phase in evaporating droplet suspensions of CNCs was discovered, suggesting complex boundary interactions are present that depend strongly on the local particle concentration. Finally, the insight gained here can guide strategies to obtain tunable particle orientation patterns.

2. Materials and methods

2.1. Cellulose nanocrystal preparation

CNCs were purchased from The University of Maine Process Development Center (Lot # 2018-FPL-CNC-126) as a concentrated gel, 10.3 wt% solids and 1.1 wt% Sulfur on dry CNC Sodium form. CNCs were diluted to 0.1 – 3.9 wt% with deionized water and stirred at 600 rpm for 30 min followed by an additional 30 min bath sonication (Branson 5800 using the high power setting). Prior to droplet casting, CNC suspensions were bath sonicated for 10 min.

2.2. Cleaning of glass substrates and sample preparation

A 1 wt% aqueous solution of Alconox detergent powder (Alconox Inc.) in deionized water (Millipore Direct-Q 3 UV, 18.2 MΩ·cm) was prepared for cleaning glass slides. The solution was degassed in an ultrasonic bath (Branson 3510 Ultrasonic Cleaner) for 30 min at 45 °C. Glass microscope slides (Thermo Scientific), measuring 75 mm × 25 mm, were then submerged into the cleaning solution and subjected to bath sonication for 10 min at 45 °C. The treatment was followed by an additional ultrasonic treatment and rinsing with deionized water. Finally, the cleaned glass slides were dried under nitrogen flow and cut with a diamond-tipped glass cutter into 37.5 mm × 25 mm pieces. Rain-X cleaned slides were prepared following the manufacturer's instructions. Accordingly, slides were rinsed in DI water and subsequently wiped with Kim wipe until dry, Rain-X was sprayed on another Kim wipe and was used to thoroughly wipe the surface of the glass slide. Finally, the slides were dried once more with a Kim wipe before testing.

Droplets, 0.25 or 0.5 µL, of aqueous CNC suspensions ranging in concentration from 0.1 to 3.9 wt% were subsequently placed on cleaned glass slides loaded on the PLM or in a 50 mm polystyrene Petri dish for AFM samples. The Petri dishes were covered with polystyrene lids that were perforated in the center with a hole of approximately 1 mm in diameter, and the droplets was allowed to dry overnight.

2.3. Polarized light microscopy

Polarized light microscopy (PLM) experiments employed a Zeiss Axioskop 40 A POL, equipped with a 530 nm first-order retardation plate. The polarizer and analyzer were oriented in east–west and north–south direction, respectively. The first-order retardation plate was inserted so that its slow axis was oriented northeast–southwest and its fast axis northwest–southeast. Images were recorded with a Canon EOS 20D digital single-lens reflex camera (8.2 megapixels) mounted onto the microscope. Time-resolved PLM videos were recorded with an Omax A3518003 digital reflex camera (18 megapixels) with a 0.5x microscope adapter for mounting. Videos, 4x magnification, were initiated immediately before droplets were pipetted on cleaned glass slides. Once placed, the microscope stage was slightly repositioned to ensure capture of the droplets. Recording was manually terminated after evaporation was complete.

2.4. Atomic force microscopy

Atomic force microscopy (AFM) was performed with an Asylum Research MFP 3D mounted onto an Olympus IX 71 inverted fluorescence microscope. For images of CNCs, 100 µL of a 0.001 wt% aqueous suspension of CNCs was spin coated (3000 rpm, 1 min) onto an aqua regia-cleaned glass slide. The sample was scanned in intermittent contact mode in air, using Nanoworld SSS-NCH SuperSharp Silicon probes (nominal tip radius: 2 nm). Dried droplets were scanned in intermittent contact mode in air, using Olympus OMCL-AC200TS-*R*3 probes (nominal tip radius: <10 nm, and nominal spring constant: 9 N m^{-1}) with 512 data points per line as well as 512 lines per scan following the CSA Z5100-17 standard [28].

2.5. Finite element analysis

A 2.0 µL, sessile, single-phase water droplet was modeled with the finite element method in COMSOL Multiphysics®. The system was allowed to evaporate in air at 23.5 °C following Fick's second law of diffusion in three dimensions. Fluid and heat transport were accounted for utilizing Cauchy's momentum equation and the equation of energy derived from first principles. A deforming mesh captured the change in volume with time in correspondence with the prescribed evaporation rate. To relate the pure fluid to the suspended media, a concentration-dependent viscosity correlation, given by Li et al., was implemented for CNCs to treat the fluid as a continuum [29]. Detailed discussion of the underlying equations of the model is available in the **Supporting Information (SI)**. The rotational Péclet numbers were calculated from the shear rate the likelihood of flow-induced particle orientation.

The simulations were performed using a cluster of Intel® Xeon® 2 × E5-2680v3 @ 2.5 GHz CPUs with 192 cores and 128 GB RAM @ 2133 MHz and were completed in 1030 CPU hours (Advanced Research Computing, Blacksburg, VA).

3. Results and discussion

In previous experiments, we analyzed the evaporation of sessile droplets of a 0.76 wt% aqueous suspension of CNCs in air after inkjet-printing onto an untreated glass slide [26]. We observed coffee-ring deposition near the periphery of the droplet which is common for droplets of colloidal suspensions having a pinned contact line [2,3]. We analyzed the resulting coffee-rings by atomic force microscopy (AFM), Figure S1, and polarized light microscopy (PLM), Figure S2. Further investigation on the influence of attractive electrostatic interactions between a positively charged substrate, cleaned with aqua regia, and negatively charged CNCs showed particle deposition in the center of the droplet in addition to the coffee-ring [26]. Notably, PLM of these droplets revealed a Maltese cross interference pattern indicating the deposited CNCs developed some degree of anisotropy in the particles comprising the coffee-ring.

3.1. Concentration-dependent CNC orientation

To investigate parameters governing the orientation of CNCs post-evaporation, the spatial alignment of CNCs from evaporated droplet suspensions was characterized with PLM as a function of initial CNC concentration and droplet volume. Polarized light microscopy (PLM) is widely used to characterize the self-assembly of CNCs into liquid crystalline phases [6–8,22,30] and therefore was implemented to characterize the particle orientation distribution post-evaporation. Specifically, PLM with a first order full-wave retardation plate, oriented with its slow axis in the northeast-southwest direction, was inserted to identify the CNC orientation. Accordingly, CNCs observed herein, will show blue colors when their slow axis, corresponding to both the cellulose chain direction and the long axis of the crystal [17], aligns in the northeast-southwest direction [30–32]. Yellow colors indicate the slow axis of the CNCs are oriented northwest-southeast, parallel to the fast axis of the wave plate [30–32]. In Figure 1, 0.25 and 0.5 μL droplets of 0.1 – 3.9 wt% (0.07 – 2.7 vol%) CNC suspensions were deposited in triplicate via micropipette on Alconox-cleaned glass slides. Alconox was implemented as the cleaning agent to reduce the effect of electrostatic interactions from the substrate on the resulting particle depositions. The droplet radius, Fig. 1b, was found to be independent of CNC concentration due to rapid contact line pinning after the initial spreading of the droplet during placement. Notably, outside of the 0.1 wt% CNC suspension, the width of coffee-rings was largely independent of CNC concentration. This suggests the droplet depins from the coffee-ring and may not maintain its pinned contact line throughout the entirety of evaporation. Likely, the 0.1 wt% CNC suspension deposited the large majority of is particles at the contact line before depinning resulting in negligible particle deposition within the droplet's center.

CNCs in suspension have been observed to form an anisotropic phase above a critical concentration, 1.8 wt%, supporting information Figure S3, for the CNCs used in this work [33]. While birefringence in CNCs is inherent to their crystalline structure, it is not detectable under PLM at low CNC concentrations due to the resolution limitations of optical microscopy [17]. In stable suspensions, CNC concentration determines the proximity of nanoparticles to one another which leads to the development of ordered structures that are detectable under PLM after sufficient time for reorganization and phase separation [15,16,33]. Here, birefringence from dried sessile droplets of CNC suspensions is observed even when the initial concentration is below the critical anisotropic phase transition concentration. This suggests CNCs are concentrated as they are entrained to the contact line such that ordered structures can be resolved under PLM. CNC confinement against the contact line likely results in the development of an anisotropic phase which is oriented parallel to the edge of the droplet as illustrated in Fig. 1. Finally, we expect the local CNC concentration in the deposit to be greater than or equal to the anisotropic phase transition concentration as these particles are kinetically limited in their ability to reorganize after deposition as compared to CNC suspensions which equilibrate to thermodynamically stable liquid crystalline order [34].

3.2. Time-dependent CNC orientation

Time-resolved PLM, supporting information: Droplet Evaporation Video 1, during evaporation confirms the maximal coffee-ring width as a result of the contact line depinning. Evaporation of droplets of CNCs suspensions on Alconox-cleaned glass thus proceed in a bimodal fashion. Initially, the contact line is pinned until remaining suspended particle concentration has dropped below a threshold to continue pinning the droplet [35,36]. After depinning, the contact line recedes until evaporation is complete and the remaining suspended particles are deposited within the central region of the droplet.

Crucially, the switch to a dynamic contact line mid-evaporation leads to a change in the orientation of deposited CNCs within the center of the droplet as observed in snapshots of time-resolved PLM, supporting information: Droplet Evaporation Video 1 and Fig. 2. Radially oriented CNCs near the contact line are initially observed, in Fig. 2a, as a result of the droplet wetting the surface of the glass slide immediately following its placement. As PLM effectively represents a thickness-averaged orientation map and cannot resolve individual CNCs, it is understood that the orientation reported herein may vary throughout the deposit thickness. Ultimately, the bulk of CNCs at the indicated locations are expected to exhibit the reported orientation measured via PLM. Droplets deposited on Alconox-cleaned glass typically develop a pinned contact line after placement and do not tend to wet in this manner which may have occurred as a result of chemical inhomogeneities on the glass surface after cleaning. Thus, an initial CNC orientation parallel to the contact line was detected in the majority of droplets deposited in this work.

After the formation of the coffee-ring, Fig. 2b illustrates a change in CNC orientation after the onset of depinning is identified. Accordingly, CNCs can be seen ordering radially prior to deposition and near the receding contact line, highlighted by the shift in color patterns at the interior of the coffee ring and pointed out by blue and yellow ar-

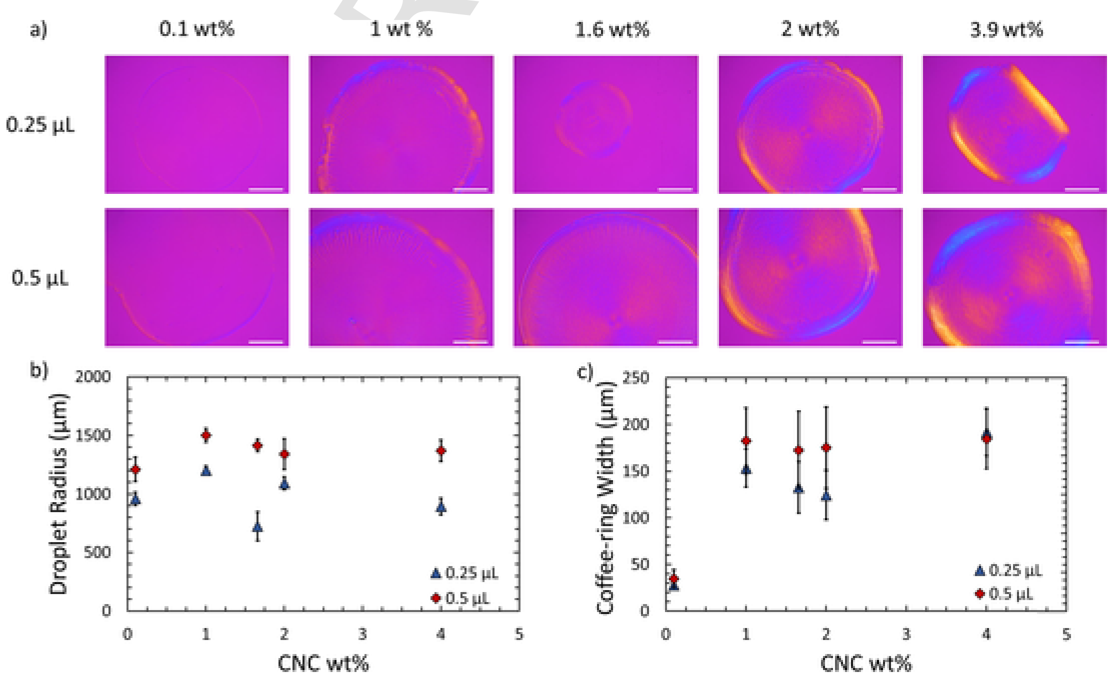

Fig. 1. a) PLM of droplet suspensions of CNCs with initial concentrations ranging from 0.1 to 3.9 wt% with initial volumes of 0.25 μL (top) and 0.5 μL (bottom) viewed with a first order full wave retardation plate, scale bar = 500 μm, b) droplet radius, and c) coffee-ring width as a function of initial CNC concentration and volume.

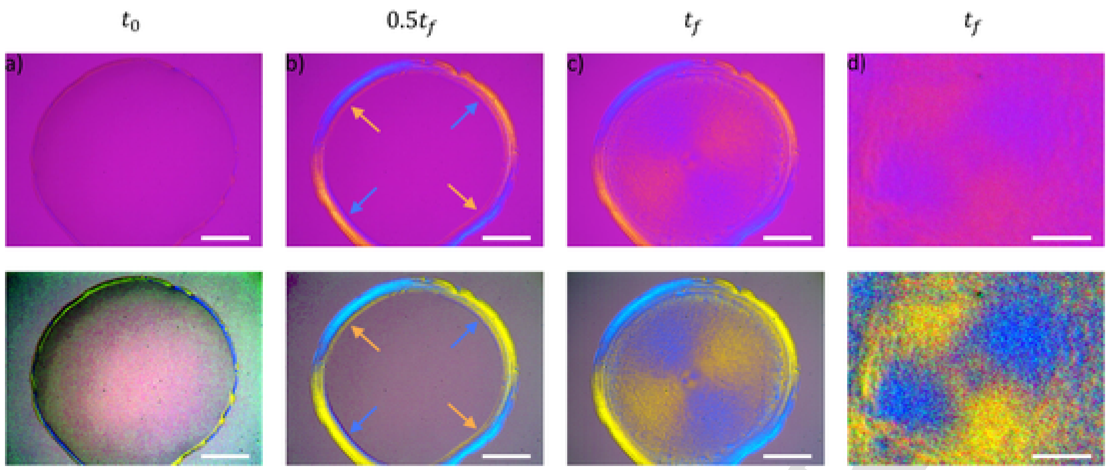

Fig. 2. Snapshots of a 0.25 μL droplet of a 2 wt% CNC aqueous suspension evaporating on an Alconox-cleaned glass slide. Time points are observed after intial deposition, a) $t = 10\,s$, halfway through evaporation, b) $t = 82.5\,s$ where blue and yellow arrows highlight local changes in orientation, c) after evaporation completes, $t = 167\,s$, and d) close up images of the center of the final deposits. The bottom images were enhanced to highlight the blue and yellow regions which are indicative of CNC alignment. a-c) Scale bar = 500 μm and d) 50 μm. (For interpretation of the references to color in this figure legend, the reader is referred to the web version of this article.)

rows in Fig. 2b. As the particles are driven to moving boundary, an intermediate phase develops with elevated viscosity due to the locally increased CNC concentration [37]. Further, the elevated concentration increases the relative strength of van der Waals and electrostatic forces between CNCs which contribute to their alignment [15]. This phenomenon illustrates the importance of local particle concentration on the evolution of the spatial distribution of particle arrangements. Ultimately once evaporation is complete, these CNCs arrange in coordination with their tangentially-oriented neighbors in Fig. 2c. As the contact line depins, tangential orientation is observed until evaporation nears completion at the center of the droplet. Here, we observed deposition of radially aligned particles at the outer edge of the center that then tangentially align near the center at certain concentrations. While tangential alignment of CNCs in evaporating droplets has been previously reported [8], this is the first demonstration of radially aligned CNCs following evaporation-induced self-assembly indicating droplet-based deposition can provide tunable orientation of rod-shaped particles. In this central region, the radial particle alignment developed near the dynamic contact line is maintained after evaporation completes. A distinct 90° rotation of CNCs deposited in the center of the droplet can be observed for initial concentrations greater than 1 wt% as evidenced by alternating blue and yellow colors progressing radially outward from the droplet center in Fig. 2c. Finally, the centermost CNCs, illustrated in Fig. 2d, reverted to a tangential alignment after deposition.

The spatial distribution of aligned CNCs after evaporation may depend on time-dependent variations in local CNC concentration as particles are removed from the suspension once deposited. The schematic in Fig. 3 illustrates the evolution of CNC orientation as a function of time as observed via time-resolved PLM and is clearly highlighted in supporting information: Droplet Evaporation Video 1. The surface tension torque [12,27], generated through the desire for CNCs to minimize the capillary energy [38,39], acting to rotate CNCs parallel to a static contact line is aided by the entrainment of new solids to the air–water interface. Additional particles are not only rotated through the effects of surface tension, but also through the hydrodynamic force generated from evaporation-induced radially outward flow [2,3] acting on rod-shaped particles impinging against a fixed boundary. Together, these effects lead to the initial formation of a coffee-ring of tangentially-oriented CNCs, Fig. 3a. Once the contact line begins to recede, Fig. 3b, an end of a CNC affixed to the contact line could trail the inward motion of the contact line and align radially. Coupled with the inherent tendency of CNCs to align with their long axis parallel, with a slight twist [32], to adjacent CNCs, a radial alignment in the vicinity of the dynamic contact line is achieved. Critically, at this stage, there is no longer a sufficient influx of additional CNCs to the boundary to create particle collisions that would otherwise rotate the CNCs parallel to the contact line. Once the contact line continues past the particles, the CNCs are able to relax into a more thermodynamically stable configuration [32] until the water between the CNCs evaporates sufficiently past the gel point. During this time, CNCs reorganize from a radial to tangential alignment. Next, near the center, Fig. 3c, the remaining CNC concentration inside the droplet has continued to decrease. Once CNCs are deposited in this domain, they may no longer feel the effects of their neighbors and will instead maintain the alignment prescribed by the receding contact line. Finally, if CNCs remain suspended in the droplet, Fig. 3d, the geometric constraints induced by the shrinking droplet begin to restrict the orientation once again to a tangential orientation.

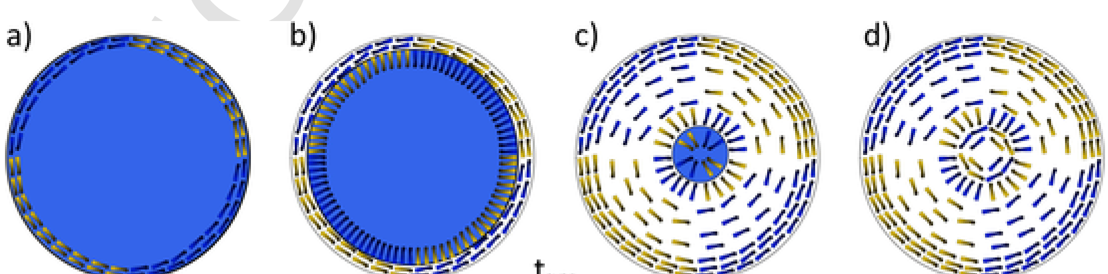

Fig. 3. Schematic depicting the progression (a → d) of CNC alignment during evaporation. a) Tangentially aligned CNCs in the coffee-ring. b) Radially aligned CNCs during contact line motion. c) CNCs from the previous step reorganize to a tangential arrangement and radially aligned CNCs are deposited near the center. d) Evaporation is complete with tangentially aligned CNCs in the center of the deposit. Dashed lines indicate the initial contact line and the blue circle shows the progression of the current droplet shape. (For interpretation of the references to color in this figure legend, the reader is referred to the web version of this article.)

To supplement the thickness-averaged orientation, illustrated with PLM, the surface topography of CNC deposits was investigated post-deposition via AFM. Height profiles, Fig. 4, were measured in four regions of the CNC deposits to compare with transition regions identified in Fig. 3: the edge, midpoint, a region just outside the center, and the center of each deposit. The northeast edge of the coffee-ring of the sample from Fig. 2 depicts tangentially oriented CNCs, Fig. 4d. The distinction between the orientation characterized from PLM and AFM is evidenced by the local change in orientation around two dust particles present in Fig. 4d. The dust particles on the surface of the coffee-ring disrupt the particle orientation leading to local deviations from tangential alignment not seen through PLM. This reinforces the ability of PLM to analyze overall bulk orientation but not necessarily individual particle orientation. Moving southwest towards the center of the droplet, CNCs in middle of the deposit are observed with a tangential orientation, Fig. 4c. Continuing near the center, Fig. 4b, orientation begins to transition to a radial alignment. Here, particles in the northeast remain tangential, yet particles nearer the center of the deposit, southwest corner, are aligned radially. Particles radially oriented in the southwest corner of Fig. 4b and northeast corner of Fig. 4a transition to a final tangential alignment in the center, as observed in the southwest corner of Fig. 4a. These results confirm the thickness-averaged orientation from PLM as well as the evolution of orientation illustrated in Fig. 3, suggesting that the bulk orientation evaluated from PLM is valid within the limits of detection for the optical technique.

3.3. Rotational Péclet number analysis

Appreciating the desire to deposit CNCs in a preferential direction, it is important to understand whether hydrodynamic shear contributes to CNC orientation post-evaporation. One might suggest that shear forces acting on the nanoparticles during their entrainment to the boundary act to rotate CNCs in the flow direction, similar to many reported shear alignment techniques and given the apparent radial alignment observed near the air–water interface during contact line recession [21,40,41]. Thus, to investigate the development of nanoparticle alignment resulting in the final CNC orientation on the substrate, computational fluid dynamic analysis was performed to analyze the impact of droplet hydrodynamics on particle alignment in evaporating sessile droplets. The effects of surface tension and convection in both the droplet and surrounding medium were considered due to their substantial impact on flow behavior. Particle interactions were approximated

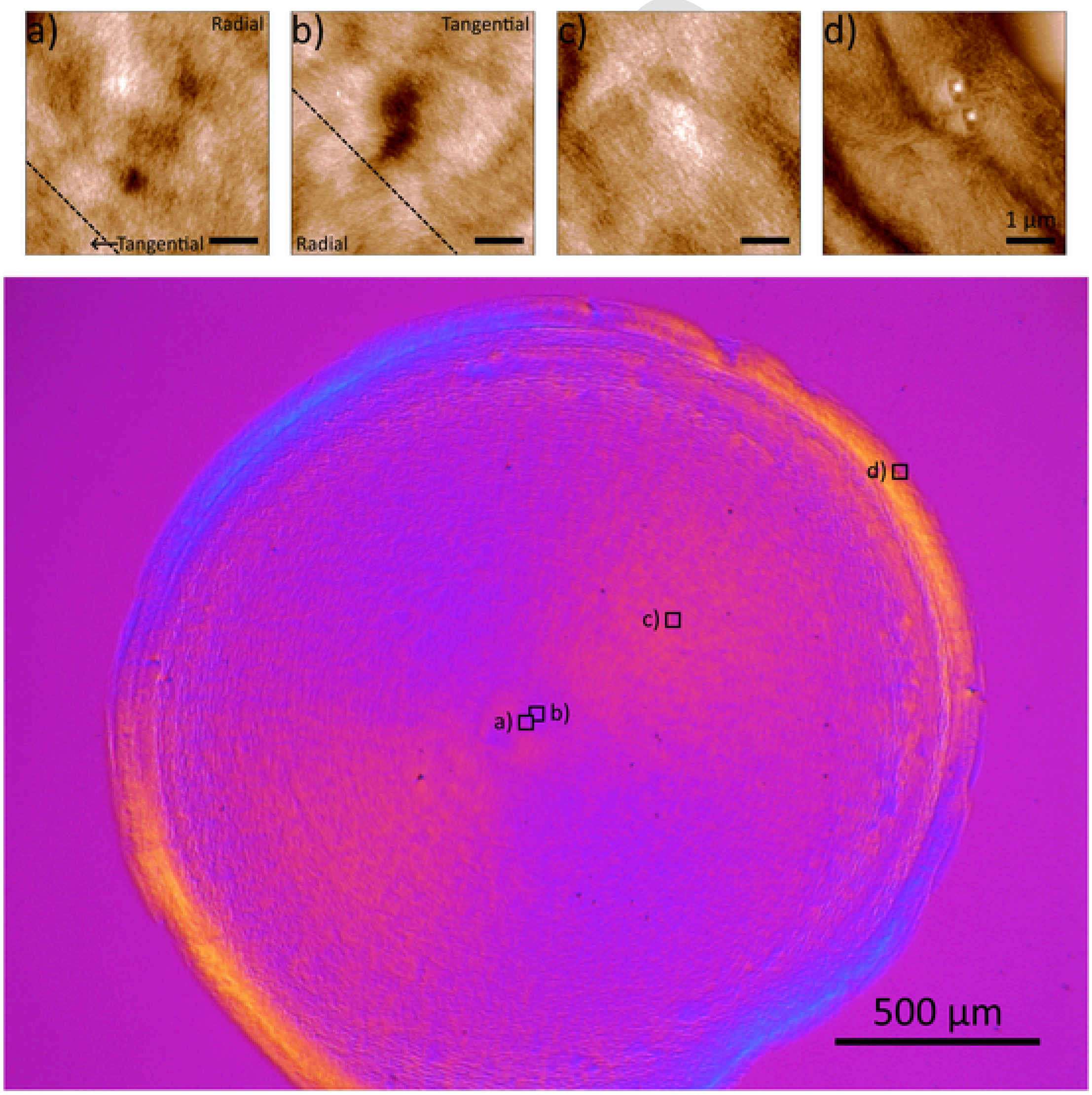

Fig. 4. AFM height profiles of a 0.25 µL droplet of a 2 wt% CNC aqueous suspension dried on an Alconox-cleaned glass slide. AFM profiles within a 5 µm × 5 µm area are depicted from four regions of the droplet: a) the center of the deposit, b) a region just outside the center, c) midpoint, and d) the edge. Corresponding regions where the height profiles were measured are highlighted in boxes on the PLM image and are enlarged for clarity to represent 40 µm × 40 µm locations.

through a concentration-dependent viscosity model, but the particles and their interactions were not explicitly and individually represented outside of a bulk empirical viscosity model. Therefore, the proposed model may capture the effects of evaporation-induced convection, but not individual particle deposition events.

We focused our investigation on the impacts of hydrodynamic forces and Brownian motion on the alignment of nanoparticles in evaporation induced flows. A concentration-dependent viscosity model was implemented to decouple the multiple levels of interaction between continuum and particle dynamics. A fundamental representation of the viscosity for rigid rod-like particle suspensions could be implemented through the Krieger-Dougherty [42] or Doi-Edwards [43] models; however, these are not representative of concentrated suspensions $n > \frac{1}{dL^2}$ which are present at the late stages of the evaporation process where particle–particle interactions become dominant. Therefore, the empirical relationship proposed by Li et al. for particle concentrations from 0.25 to 1.5 wt% was employed [29]:

$$\eta_{sp} = 24832c_{CNC}^2 + 283.8c_{CNC} \tag{1}$$

where η_{sp} is the specific viscosity of the suspension of CNCs in water and c_{CNC} is the concentration of CNCs in the suspension in g mL^{-1}. Comparison of this model to other rheological characterization of aqueous CNC suspensions provides reasonable agreement of this model up to approximately 6 wt% as illustrated in Figure S5 [37].

Hydrodynamic-induced alignment was studied through the rotational Péclet number described by Willenbacher and Georgieva, Eqs. (2) and (3), which expresses the extent to which hydrodynamic forces overcome Brownian motion in controlling alignment [44].

$$P\acute{e}_{rot} = \tau_{rot}\dot{\gamma} \tag{2}$$

$$\tau_{rot} = \frac{8\pi\eta_s a^3}{3k_B T(ln2r_p - 0.5)} \tag{3}$$

where $\dot{\gamma}$ is the shear rate, τ_{rot} is the rotational relaxation time, η_s is the solvent viscosity, a is the length of the semi-major axis of a prolate spheroid representing the rod-like particle, k_B is the Boltzmann constant, T is temperature in Kelvin, and r_p is the aspect ratio of the particle. Rotational Péclet numbers greater than unity describe systems in which shear induced flow alignment dominates. Alignment in systems with Péclet numbers less than unity is governed by Brownian motion acting to randomize the orientation of particles. The rotational relaxation time was evaluated with Eq. (3) and was found to be 2.1 × 10^{-4} s for CNCs at 23.5 °C used in this work, corresponding to a solvent viscosity of 1 mPa s, CNC length of 123 nm, and CNC aspect ratio of 5.1. Therefore, shear rates greater than 4.73 × 10^3 s^{-1} should lead to hydrodynamic flow alignment.

Rotational Péclet numbers were calculated from Eq. (2) for an evaporating water droplet and CNC suspension droplet over the course of evaporation at 23.5 °C, Figure S6 and were found to be constant with respect to time and droplet location in room temperature evaporation. The Rotational Péclet number, 3.2 × 10^{-12}, is very significantly less than unity suggesting that Brownian motion dominates, and particles remain in their initial isotropic (unaligned) orientation as they are carried to the edge of the droplet. The hydrodynamic forces calculated here are without specific particle interaction contributions and are not sufficient to induce significant orientation at 23.5 °C. Particles contained within the suspensions may be entrained in the flow and thus deposited at the edge of the droplet but would not necessarily develop long-range preferential orientation without the effects of additional interactions. Thus, the bulk of CNC orientation occurs as a result of contact line dynamics, surface tension, and interparticle interactions, supporting Mashkour's [12,27] advances in this space.

3.4. Orientation in liquid crystalline CNC suspensions

The absence of hydrodynamic alignment was confirmed experimentally, in triplicate, through the characterization of aqueous suspensions of anisotropic CNCs evaporating on hydrophilic substrates. These droplets initially formed an anisotropic phase in suspension as evidenced by their initial configuration immediately after deposition, Fig. 5 t_0. Changes in orientation were then investigated during evaporation, Fig. 5 t_0-t_f. Isolation of the anisotropic phase of a 3.9 wt% aqueous suspension of CNCs was carefully extracted after leaving the suspension to phase separate into its isotropic and anisotropic phases for one week [15]. The isotropic-anisotropic transition was found to be 1.8 wt% for these CNCs, Figure S3. While the CNCs were exposed to shear stress during the withdrawal and ejection from the micropipette, the droplets maintained a significant order after placement which was visible through PLM as shown in Fig. 5. Coupled with time-resolved PLM, supporting information: Droplet Evaporation Video 2, these results illustrate ordered CNCs migrating to the contact line during evaporation. In support of calculations of the rotational Péclet number, local particle orientation is unperturbed by the shear flow. Additionally, clusters of CNCs migrating to the contact line are observed rotating to match the tangential orientation of their neighbors upon their approach, highlighting the role of interparticle interactions governing the orientation of structured domains of deposited CNCs.

3.5. CNC orientation on hydrophobic substrates

Finally, to analyze the role of the contact line on the evolution of CNC orientation in drying droplets, we explore the effects of hydrophobicity on the ensuing particle deposition in triplicate as depicted in Fig. 6 and supporting information: Droplet Evaporation Video 3. Hydrophobic droplets commonly evaporate with a receding contact line to maintain their contact angle with the substrate throughout evaporation and therefore serve as an excellent technique to observe the role of contact line motion in the development of CNC orientation [1,45]. We expect the contact line to recede in droplets containing negatively-charged suspended CNCs, Fig. 6a–c, until the CNC concentration exceeds the gel point [34].

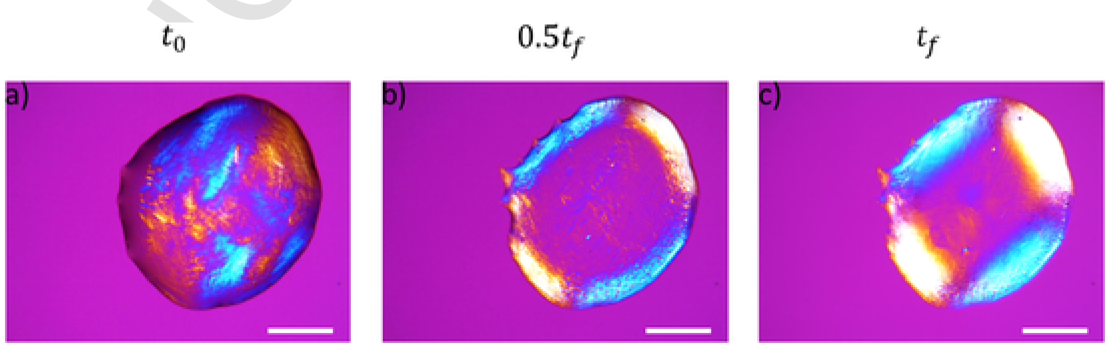

Fig. 5. Snapshots of a 0.25 μL droplet of an initially anisotropic 3.9 wt% CNC aqueous suspension evaporating on an Alconox-cleaned glass slide. Time points are observed after intial deposition, a) t = 9 s, halfway through b) t = 132.5 s, and after evaporation completes c) t = 265 s. Scale bar = 500 μm.

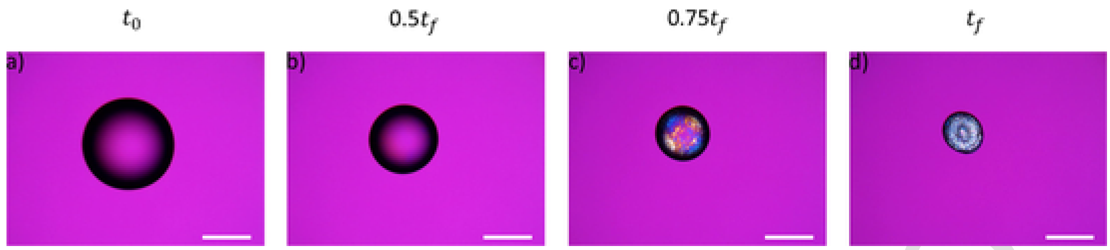

Fig. 6. Snapshots of a 0.5 μL droplet of 2 wt% CNC aqueous suspension evaporating on a Rain-X-cleaned glass slide. Time points are observed after intial deposition, a) t = 5 s, halfway through b) t = 225 s, c) $t = 330\ s$, and after evaporation completes d) t = 445 s. Scale bar = 500 μm.

The initial stages of evaporation on a hydrophobic substrate are notably different from hydrophilic surfaces. The near instantaneous formation of CNC alignment near the contact line, as shown previously, is not observed. In fact, ordered domains of CNCs are not visibly apparent under PLM until nearly three-quarters of the evaporation time has elapsed, Fig. 6c. While tangentially aligned CNCs are observed at this time, their ultimate configuration, Fig. 6d, is difficult to discern. Once gelation is established and the droplet remains fixed, evaporation proceeds to evolve the remaining water within the CNC network. The removal of the interstitial water results in a collapse in the height of the droplet as well as a reduction in inter-CNC spacing [46]. This results in a semi-ordered deposit, likely comprised of many tactoids of aligned regions of CNCs, but lacks the regular arrangement of nanoparticles following evaporation on a hydrophilic substrate. In this case, CNCs are not given the opportunity to deposit at a pinned contact line during evaporation or cooperatively develop a tangentially aligned structure in the proximity of the contact line. Instead, the restricted time for reorganization after gelation and before solvent removal reduces the free volume leading to severely hindered particle mobility and ultimately smaller domains of ordered structures.

4. Conclusions

Time-resolved polarized light microscopy provides a powerful tool for the characterization of optically anisotropic nanomaterials which dynamically develop ordered structures larger than the wavelength of visible light. These structures can be identified in real-time thereby illuminating complex structural interactions, traditionally observed only in steady state flow or *ex post facto*. Additionally, the onset of birefringence observed via PLM captures local CNC concentration gradients that induce preferential orientation as a function of the kinetics associated with evaporation and droplet depinning. The evolution of particle orientation throughout the droplet is highly dependent on the interfacial surface tension and cooperative interactions between CNCs but was generally not found to be a result of flow-induced shear alignment. The surface tension acts to aid the initial CNC rotation coincident to the contact line which defines the orientation for particles deposited within the coffee-ring. Competition between electrostatic repulsion and capillary flow was observed as a function of the local particle concentration dynamically changing during evaporation leading to changes in the observed orientation of deposited CNCs. We present the deposition of highly ordered ring structures from dilute CNC suspensions which can be varied in size through the droplet volume as well as new evidence for radially aligned CNCs in the center of the deposit. The deposited orientation and arrangement of CNCs differs from the behavior of cylindrical particles which tend to develop end-to-end chains [38,47]. Further, in comparison to previous reports that observed either tangential alignment in drying droplets [12,27,32] or cholesteric ordering [48–50] in cast films, our observations of radial alignment show that the orientation of deposited rod-like nanoparticles can be controlled via low-cost energy-efficient droplet evaporation. A comprehensive analysis of the concentration- and shear rate-dependent nature of viscosity and interparticle interactions, especially in highly concentrated systems, is in progress to further elucidate parameters associated with the development of highly ordered, radial or tangential, structures applicable to the next generation of spatially and directionally ordered systems of anisotropic nanomaterials.

Funding sources

Department of Education GAANN Fellowship program (P200A180016). USDA Cooperative State Research, Education and Extension Service (2005-35504-16088).

CRediT authorship contribution statement

Cailean Q. Pritchard: Conceptualization, Methodology, Investigation, Validation, Formal analysis, Writing - original draft. **Fernando Navarro:** Methodology, Investigation. **Maren Roman:** Conceptualization, Resources, Supervision, Writing - review & editing. **Michael J. Bortner:** Conceptualization, Resources, Supervision, Project administration, Writing - review & editing.

Declaration of Competing Interest

The authors declare that they have no known competing financial interests or personal relationships that could have appeared to influence the work reported in this paper.

Acknowledgements

The authors gratefully acknowledge generous scholarship support for F. N. by the Mexican department of Education (SEP) through its Professional Development for Teachers program (PROMEP). This project was further supported by the National Research Initiative of the USDA Cooperative State Research, Education and Extension Service, grant number 2005-35504-16088. We thank OMNOVA, Inc. and Tembec, Inc. for supplying the cellulose pulp used in this work. Additionally, we would like to acknowledge the Department of Education GAANN Fellowship program (P200A180016) for their funding and support for this work.

Appendix A. Supplementary material

Supplementary data to this article can be found online at https://doi.org/10.1016/j.jcis.2021.06.069.

References

[1] A.J. Petsi, V.N. Burganos, Evaporation-induced flow in an inviscid liquid line at any contact angle, Phys. Rev. E – Stat., Nonlinear, Soft Matter Phys. 73 (2006) 1–9.
[2] R.D. Deegan, O. Bakajin, T.F. Dupont, G. Huber, S.R. Nagel, T.A. Witten, Capillary flow as the cause of ring stains from dried liquid drops, Nature 389 (6653) (1997) 827–829.
[3] R.D. Deegan, O. Bakajin, T.F. Dupont, G. Huber, S.R. Nagel, T.A. Witten, Contact line deposits in an evaporating drop, Phys. Rev. E Stat. Phys. Plasmas Fluids Relat. Interdiscip. Topics 62 (1) (2000) 756–765.
[4] M. Maillard, L. Motte, M.P. Pileni, Rings and Hexagons Made of Nanocrystals, Adv. Mater. 13 (3) (2001) 200–204.
[5] H. Hu, R.G. Larson, Marangoni effect reverses coffee-ring depositions, J Phys. Chem. B 110 (14) (2006) 7090–7094.
[6] A. Gencer, C. Schutz, W. Thielemans, Influence of the Particle Concentration and Marangoni Flow on the Formation of Cellulose Nanocrystal Films, Langmuir 33 (1) (2017) 228–234.

[7] A. Gencer, J. Van Rie, S. Lombardo, K. Kang, W. Thielemans, Effect of Gelation on the Colloidal Deposition of Cellulose Nanocrystal Films, Biomacromolecules 19 (8) (2018) 3233–3243.
[8] X. Mu, D.G. Gray, Droplets of cellulose nanocrystal suspensions on drying give iridescent 3-D "coffee-stain" rings, Cellulose 22 (2) (2015) 1103–1107.
[9] S. Ye, Q. Fu, J. Ge, Invisible Photonic Prints Shown by Deformation, Adv. Funct. Mater. 24 (41) (2014) 6430–6438.
[10] P. Saha, N. Ansari, C.L. Kitchens, W.R. Ashurst, V.A. Davis, Microelectromechanical Systems from Aligned Cellulose Nanocrystal Films, ACS Appl. Mater. Interfaces 10 (28) (2018) 24116–24123.
[11] F. Hoeng, A. Denneulin, J. Bras, Use of nanocellulose in printed electronics: a review, Nanoscale 8 (27) (2016) 13131–13154.
[12] M. Mashkour, T. Kimura, M. Mashkour, F. Kimura, M. Tajvidi, Printing Birefringent Figures by Surface Tension-Directed Self-Assembly of a Cellulose Nanocrystal/Polymer Ink Components, ACS Appl. Mater. Interfaces 11 (1) (2019) 1538–1545.
[13] E.J. Foster, R.J. Moon, U.P. Agarwal, M.J. Bortner, J. Bras, S. Camarero-Espinosa, K.J. Chan, M.J.D. Clift, E.D. Cranston, S.J. Eichhorn, D.M. Fox, W.Y. Hamad, L. Heux, B. Jean, M. Korey, W. Nieh, K.J. Ong, M.S. Reid, S. Renneckar, R. Roberts, J.A. Shatkin, J. Simonsen, K. Stinson-Bagby, N. Wanasekara, J. Youngblood, Current characterization methods for cellulose nanomaterials, Chem. Soc. Rev. 47 (8) (2018) 2609–2679.
[14] J.F. Revol, H. Bradford, J. Giasson, R.H. Marchessault, D.G. Gray, Helicoidal self-ordering of cellulose microfibrils in aqueous suspension, Int. J. Biol. Macromol. 14 (3) (1992) 170–172.
[15] C. Schutz, M. Agthe, A.B. Fall, K. Gordeyeva, V. Guccini, M. Salajkova, T.S. Plivelic, J.P. Lagerwall, G. Salazar-Alvarez, L. Bergstrom, Rod Packing in Chiral Nematic Cellulose Nanocrystal Dispersions Studied by Small-Angle X-ray Scattering and Laser Diffraction, Langmuir 31 (23) (2015) 6507–6513.
[16] J.P.F. Lagerwall, C. Schütz, M. Salajkova, J. Noh, J. Hyun Park, G. Scalia, L. Bergström, Cellulose nanocrystal-based materials: from liquid crystal self-assembly and glass formation to multifunctional thin films, NPG Asia Mater. 6 (1) (2014) 1–12.
[17] W.Y. Hamad, Cellulose Nanocrystals Properties, Production, and Applications, John Wiley & Sons Ltd (2017) 289.
[18] M. Tatsumi, F. Kimura, T. Kimura, Y. Teramoto, Y. Nishio, Anisotropic polymer composites synthesized by immobilizing cellulose nanocrystal suspensions specifically oriented under magnetic fields, Biomacromolecules 15 (12) (2014) 4579–4589.
[19] K.J. De France, K.G. Yager, T. Hoare, E.D. Cranston, Cooperative Ordering and Kinetics of Cellulose Nanocrystal Alignment in a Magnetic Field, Langmuir 32 (30) (2016) 7564–7571.
[20] P. Dhar, A. Kumar, V. Katiyar, Magnetic Cellulose Nanocrystal Based Anisotropic Polylactic Acid Nanocomposite Films: Influence on Electrical, Magnetic, Thermal, and Mechanical Properties, ACS Appl. Mater. Interfaces 8 (28) (2016) 18393–18409.
[21] M. Tatsumi, Y. Teramoto, Y. Nishio, Different orientation patterns of cellulose nanocrystal films prepared from aqueous suspensions by shearing under evaporation, Cellulose 22 (5) (2015) 2983–2992.
[22] E.D. Cranston, D.G. Gray, Birefringence in spin-coated films containing cellulose nanocrystals, Colloids Surf., A 325 (1–2) (2008) 44–51.
[23] S. Chen, G. Schueneman, R.B. Pipes, J. Youngblood, R.J. Moon, Effects of crystal orientation on cellulose nanocrystals-cellulose acetate nanocomposite fibers prepared by dry spinning, Biomacromolecules 15 (10) (2014) 3827–3835.
[24] J.N. O'Shea, J.B. Taylor, J.C. Swarbrick, G. Magnano, L.C. Mayor, K. Schulte, Electrospray deposition of carbon nanotubes in vacuum, Nanotechnology 18 (2007).
[25] H. Xin, A.T. Woolley, Directional orientation of carbon nanotubes on surfaces using a gas flow cell, Nano Lett. 4 (2004) 1481–1484.
[26] F.N. Maren Roman, Deposition of Cellulose Nanocrystals by Inkjet Printing, inn: Model Cellulosic Surfaces, ACS Publications, 2009, pp 157-171.
[27] M. Mashkour, T. Kimura, F. Kimura, M. Mashkour, M. Tajvidi, Tunable self-assembly of cellulose nanowhiskers and polyvinyl alcohol chains induced by surface tension torque, Biomacromolecules 15 (1) (2014) 60–65.
[28] Z5100-17 Cellulosic nanomaterials — Test methods for characterization, in: Atomic Force Microscopy, CSA Group: Ontario, Canada, 2017, pp 43-46
[29] M.C. Li, Q. Wu, K. Song, S. Lee, Y. Qing, Y. Wu, Cellulose Nanoparticles: Structure-Morphology-Rheology Relationships, ACS Sustainable Chem. Eng. 3 (2015) 821–832.
[30] S. Ghasemi, P. Rahimzadeh-Bajgiran, M. Tajvidi, S.M. Shaler, Birefringence-based orientation mapping of cellulose nanofibrils in thin films, Cellulose 27 (2) (2019) 677–692.
[31] M. Roman, D.G. Gray, Parabolic focal conics in self-assembled solid films of cellulose nanocrystals, Langmuir 21 (12) (2005) 5555–5561.
[32] D.G. Gray, X. Mu, Chiral Nematic Structure of Cellulose Nanocrystal Suspensions and Films; Polarized Light and Atomic Force Microscopy, Materials (Basel) 8 (11) (2015) 7873–7888.
[33] E.E. Ureña-Benavides, G. Ao, V.A. Davis, C.L. Kitchens, Rheology and Phase Behavior of Lyotropic Cellulose Nanocrystal Suspensions, Macromolecules 44 (22) (2011) 8990–8998.
[34] D.G. Gray, Order and gelation of cellulose nanocrystal suspensions: an overview of some issues, Philos. Trans. A Math. Phys. Eng. Sci. 376 (2112) (2018) 1–7.
[35] K.N. Al-Milaji, H. Zhao, Probing the Colloidal Particle Dynamics in Drying Sessile Droplets, Langmuir 35 (6) (2019) 2209–2220.
[36] M.E.R. Shanahan, Simple Theory of "Stick-Slip" Wetting Hysteresis, Langmuir 11 (3) (1995) 1041–1043.
[37] J. Liao, K.A. Pham, V. Breedveld, Rheological characterization and modeling of cellulose nanocrystal and TEMPO-oxidized cellulose nanofibril suspensions, Cellulose 27 (7) (2020) 3741–3757.
[38] M. Cavallaro Jr., L. Botto, E.P. Lewandowski, M. Wang, K.J. Stebe, Curvature-driven capillary migration and assembly of rod-like particles, Proc Natl. Acad. Sci. U S A 108 (52) (2011) 20923–20928.
[39] L. Botto, L. Yao, R.L. Leheny, K.J. Stebe, Capillary bond between rod-like particles and the micromechanics of particle-laden interfaces, Soft Matter 8 (18) (2012) 4971–4979.
[40] I. Hoeger, O.J. Rojas, K. Efimenko, O.D. Velev, S.S. Kelley, Ultrathin film coatings of aligned cellulose nanocrystals from a convective-shear assembly system and their surface mechanical properties, Soft Matter 7 (5) (2011) 1957–1967.
[41] M. Alizadehgiashi, A. Khabibullin, Y. Li, E. Prince, M. Abolhasani, E. Kumacheva, Shear-Induced Alignment of Anisotropic Nanoparticles in a Single-Droplet Oscillatory Microfluidic Platform, Langmuir 34 (1) (2018) 322–330.
[42] I.M. Krieger, T.J. Dougherty, A Mechanism for Non-Newtonian Flow in Suspensions of Rigid Spheres, Trans. Soc. Rheol. 3 (1959) 137–152.
[43] M. Doi, S.F. Edwards, The Theory of Polymer, Dynamics 391 (1988).
[44] N. Willenbacher, K. Georgieva, Rheology of Disperse Systems, in: Product Design and Engineering: Formulation of Gels and Pastes, Brockel, U.; Meier, W.; Gerhard, W., Eds. 2013, pp 7-49.
[45] D.O. Kim, M. Pack, A. Rokoni, P. Kaneelil, Y. Sun, The effect of particle wettability on the stick-slip motion of the contact line, Soft Matter 14 (47) (2018) 9599–9608.
[46] F. Jativa, C. Schutz, L. Bergstrom, X. Zhang, B. Wicklein, Confined self-assembly of cellulose nanocrystals in a shrinking droplet, Soft Matter 11 (26) (2015) 5374–5380.
[47] E.P. Lewandowski, M. Cavallaro Jr., L. Botto, J.C. Bernate, V. Garbin, K.J. Stebe, Orientation and self-assembly of cylindrical particles by anisotropic capillary interactions, Langmuir 26 (19) (2010) 15142–15154.
[48] S. Beck, J. Bouchard, G. Chauve, R. Berry, Controlled production of patterns in iridescent solid films of cellulose nanocrystals, Cellulose 20 (3) (2013) 1401–1411.
[49] J. Majoinen, E. Kontturi, O. Ikkala, D.G. Gray, SEM imaging of chiral nematic films cast from cellulose nanocrystal suspensions, Cellulose 19 (5) (2012) 1599–1605.
[50] D. Liu, S. Wang, Z. Ma, D. Tian, M. Gu, F. Lin, Structure–color mechanism of iridescent cellulose nanocrystal films, RSC Adv. 4 (74) (2014) 39322–39331.